

Forgetting to Remember: A Scalable Incremental Learning Framework for Cross-Task Blind Image Quality Assessment

Rui Ma, Qingbo Wu, *Member, IEEE*, King Ngı Ngan, *Life Fellow, IEEE*, Hongliang Li, *Senior Member, IEEE*, Fanman Meng, *Member, IEEE*, Linfeng Xu, *Member, IEEE*

Abstract—Recent years have witnessed the great success of blind image quality assessment (BIQA) in various task-specific scenarios, which present invariable distortion types and evaluation criteria. However, due to the rigid structure and learning framework, they cannot apply to the cross-task BIQA scenario, where the distortion types and evaluation criteria keep changing in practical applications. This paper proposes a scalable incremental learning framework (SILF) that could sequentially conduct BIQA across multiple evaluation tasks with limited memory capacity. More specifically, we develop a dynamic parameter isolation strategy to sequentially update the task-specific parameter subsets, which are non-overlapped with each other. Each parameter subset is temporarily settled to *Remember* one evaluation preference toward its corresponding task, and the previously settled parameter subsets can be adaptively reused in the following BIQA to achieve better performance based on the task relevance. To suppress the unrestrained expansion of memory capacity in sequential tasks learning, we develop a scalable memory unit by gradually and selectively pruning unimportant neurons from previously settled parameter subsets, which enable us to *Forget* part of previous experiences and free the limited memory capacity for adapting to the emerging new tasks. Extensive experiments on eleven IQA datasets demonstrate that our proposed method significantly outperforms the other state-of-the-art methods in cross-task BIQA. The source code of the proposed method is available at <https://github.com/maruiperfect/SILF>.

Index Terms—Cross-Task BIQA, relevance-aware incremental learning, task relevance, parameter reuse, additional task learning.

I. INTRODUCTION

BLIND image quality assessment (BIQA) aims to evaluate the perceptual quality of an image where the prior knowledge of its reference image and distortion type is unavailable. Due to the absence of pristine reference and the unpredictability of various distortions in the open environment, BIQA is highly desired in many practical applications, such as image quality monitoring, camera tuning, network adaptation, and so on. Recently, many BIQA methods [1]–[10] have achieved impressive performance in diverse task-specific evaluations, including synthetic, authentic, and enhancement distortion

evaluation tasks. However, in practical applications, the distortion artifacts and evaluation criteria may keep changing with the task scenario, which brings new demand for cross-task BIQA. More specifically, we require a general-purpose model to sequentially learn the perceptual preference across different types of BIQA tasks, which mimics the continual knowledge accumulation of the human, as shown in Fig. 1.

The most straightforward approach is to train a separate model for every new task. Despite the best performance for the cross-task scenario, this method requires a lot of storage space and computing resources, which is challenging to apply in practice. Another solution is to use only one static model and fine-tune the old model to adapt to new tasks, whose storage and computation overhead would not grow with the increasing new tasks. Unfortunately, the model tends to forget old knowledge after learning a new task. This phenomenon, known as catastrophic forgetting [11], where the model tends to change the weights necessary for previous tasks to adapt to new tasks, occurs when the model learns multiple tasks sequentially.

Recently, several pioneering works [12]–[14] have been proposed to address the catastrophic forgetting problem in cross-task BIQA. Zhang et al. [12] propose a simple yet effective method for continually learning BIQA models by training task-specific batch normalization parameters for each task while keeping all pre-trained convolution filters fixed. Based on a shared backbone network, Zhang et al. [13] add a prediction head for a new dataset and enforce a regularizer to allow all prediction heads to evolve with new data while resisting old data catastrophic forgetting. Limited by the hard parameter sharing of the backbone, these methods [12], [13] are hard to apply to the BIQA tasks with significant differences. LIQA [14] employs a generator conditioned on the distortion type and the quality score to generate pseudo features, which serve as a memory replayer when learning new tasks. Despite the success of adapting to significantly different BIQA tasks, LIQA requires additional computational and memory resources for generating and reusing the paired pseudo features and labels. Unlike the aforementioned hard parameter sharing and replay strategies, in our previous work [15], we proposed a remember and reuse network (R&R-Net) to separate all model parameters into predefined subsets according to the specified task capacity. This rigid parameter

This work was supported in part by the National Natural Science Foundation of China under Grant 61971095, Grant 61831005, and Grant 61871087. (Corresponding authors: Qingbo Wu; Fanman Meng.) The authors are with the School of Information and Communication Engineering, University of Electronic Science and Technology of China, Chengdu 611731, China (e-mail: ruima@std.uestc.edu.cn; qbwu@uestc.edu.cn; knngan@cuhk.edu.hk; hlli@uestc.edu.cn; fmmeng@uestc.edu.cn; lfxu@uestc.edu.cn).

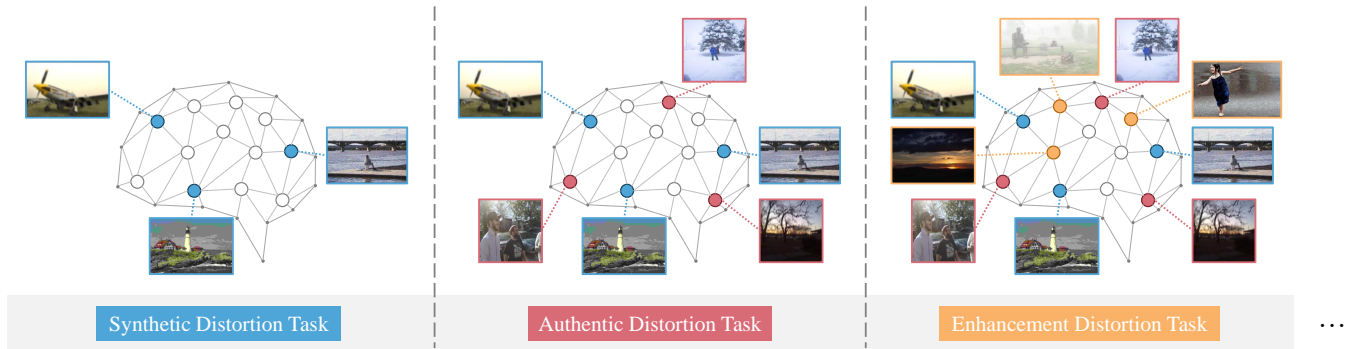


Fig. 1. Cross-task blind image quality assessment process. The model sequentially evaluates different types of BIQA tasks. Zoom in to observe better the distorted details of the images for various tasks.

isolation strategy efficiently avoids catastrophic forgetting with limited memory. However, in the meantime, it also prevents R&R-Net from learning additional tasks which exceed the specified task capacity.

This paper extends R&R-Net with the dynamic parameter isolation strategy and scalable memory unit. Specifically, we set two pruning ratios for each preset task: the first and second pruning ratios. The first pruning aims to release the redundant parameters of the current task for subsequent preset tasks. The second pruning enables the scalability of our model to learn additional tasks that exceed the preset task capacity. After two prunings, we obtain two candidate models corresponding to the current task, which we call the maximum and minimum models. During fine-tuning, we train the two models alternately. In practical applications, if there are no additional tasks, the preset tasks can employ their corresponding maximum models to achieve the best performance. Otherwise, the preset tasks can exploit their related minimum models to free the memory of the scalable memory unit to learn the additional tasks. By means of negligible sacrifice on the preset tasks, our model can increase the task capacity without expanding the memory capacity.

Compared to our previous work, the additional contributions of this paper are summarized in the following:

- 1) We propose a scalable incremental learning framework (SILF). By gradually and selectively pruning unimportant neurons from previously settled parameter subsets, we develop a scalable memory unit, which enables us to forget part of previous experiences and free the limited memory capacity for adapting to emerging new tasks. In this way, we effectively extend the task capacity of the model without increasing its memory capacity.
- 2) We conduct extensive experiments to evaluate the proposed method on eleven IQA databases, including the synthetic, authentic, and enhancement distortion evaluation tasks. The results demonstrate that our proposed method significantly outperforms many state-of-the-art methods, even for the additional tasks.

The rest of this paper is organized as follows. Section II reviews the related work. Section III presents the proposed method. Section IV introduces experimental results and their analysis. Finally, Section V concludes the paper.

II. RELATED WORK

This section briefly reviews representative BIQA and incremental learning methods closely related to our work.

A. Blind Image Quality Assessment

Existing BIQA methods can be divided into opinion-aware BIQA and opinion-unaware BIQA, depending on whether opinion scores are required during the training process.

Opinion-aware BIQA methods learn regression models based on training images and subjective evaluations of the people involved to predict the perceptual quality of the test images. Traditional opinion-aware BIQA methods extract hand-crafted quality-aware features and then convert these features into quality scores employing a regression function. Natural scene statistic (NSS) based methods [16]–[23] are the most common of these methods. Some learning-based methods [24], [25], which learn features from training data, have also been developed to overcome the limitations of hand-crafted features. The convolutional neural network (CNN) has recently achieved great success in various computer vision tasks, such as image classification, object detection, and semantic segmentation. Due to its robust feature representation capabilities, the CNN-based BIQA methods [26]–[34] have shown superior prediction performance over traditional methods. Inspired by the deep residual model [35], Bare et al. [29] add two sum layers to a simple CNN network for BIQA. Bosse et al. [28] modify VGGNet [36] to learn local weights to measure the importance of the local quality of each image patch and employ weighted average patch aggregation as a pooling method. Zhang et al. [31] propose a deep bilinear CNN-based (DB-CNN) BIQA model by conceptually modeling both synthetic and authentic distortions as two-factor variations by bilinear pooling. Inspired by deep meta-learning [37], Zhu et al. [33] propose an optimization-based meta-learning method for BIQA, which applies several distortion-specific NR-IQA tasks to learn prior knowledge of multiple distortions in images.

Opinion-unaware BIQA methods do not require subjective human opinions for training. Nature image quality evaluator (NIQE) [38] extracts local features from an image and fits the feature vectors to a multivariate Gaussian model (MVG). It then predicts the quality of the test image based on the

distance between its MVG model and the MVG model learned from a corpus of new naturalistic images. Zhang et al. [39] then extend NIQE to integrated local NIQE (IL-NIQE). The IL-NIQE model extracts five types of NSS features from a collection of original natural images and then applies them to learn an MVG model of original images as a reference model for predicting the quality of the image patches. Given a test image, the model evaluates the scores of its patches separately and then employs the mean of these scores as the score of the test image. Wu et al. [40] propose a local pattern statistics index (LPSI) characterized by its good generality to various distortions. Liu et al. [41] propose natural scene statistics and perceptual characteristics-based quality index (NPQI) by investigating the human brain’s NSS and perceptual features for visual perception.

B. Incremental Learning

Incremental learning has been a long-standing research problem in machine learning, focusing on learning efficient models from sequentially arriving data. Existing incremental learning methods can be summarily grouped into the following categories: namely, regularization-based, replay-based, dynamic architecture-based, and parameter isolation-based.

Regularization-based methods introduce regularization terms into the loss function to penalize network parameter changes when learning the current task to prevent catastrophic forgetting. Learning without forgetting (LwF) [42] attempts to prevent model parameters from changing while training the current task by applying a cross-entropy loss regularized by a distillation loss [43]. Elastic weight consolidation (EWC) [44] limits the change of essential parameters for previous tasks by imposing a quadratic penalty term that encourages weights to move in directions with low Fisher information. Schwarz et al. [45] then propose online EWC (OEWC), which optimizes the EWC by reducing the cost of estimating the Fisher information matrix.

Replay-based methods store representative examples of previous tasks in a replay buffer [46]–[48] or train a generative model to generate samples of previous tasks [49]–[51]. The model is jointly trained by combining the stored data with the data from the current task. Rebuffi et al. [46] select the samples closest to the average sample of each task as the replay subset. Belouadah et al. [47] introduce second memory to store statistics of previous tasks. Another popular strategy is to train a generative adversarial network (GAN) [52]. GAN can be employed to synthesize exemplars for previous tasks. Shin et al. [49] propose a cooperative dual model architecture consisting of deep generative and task-solving models. Xiang et al. [51] propose an incremental learning strategy based on conditional adversarial networks.

Dynamic architecture-based methods adapt new incoming tasks by modifying/expanding the network structure [53]–[58]. Progressive neural networks (PNN) [53] develop a new column of the entire neural network for each task and transfer previously learned task features via lateral connections. Dynamically expandable networks (DEN) [54] expand the network capacity by the number of units required for each

task arrival. Rajasegaran et al. [57] propose a randomized path selection method called RPS-Net, which applies a randomized path selection method for each task.

Parameter isolation-based methods assign diverse parameters to different tasks to prevent catastrophic forgetting [59]–[63]. Serra et al. [60] introduce a task-based intricate attention mechanism that preserves the information of previous tasks without affecting the learning of the current task. Mallya et al. [61] propose PackNet for learning multiple tasks using iterative pruning. Ebrahimi et al. [63] propose an incremental learning formulation with Bayesian neural networks, which utilizes uncertainty predictions to conduct incremental learning. Essential parameters are either fully preserved by a stored binary mask or modified according to their uncertainty for learning new tasks.

Algorithm 1 Scalable Task Incremental Learning Algorithm

Input: Datasets: $\{\mathcal{D}_t\}_{t=1}^{n+k}$,
task capacity: n , scalable task capacity: k ,
first pruning ratios: $\mathcal{P} = \{p_1, p_2, \dots, p_n\}$,
second pruning ratios: $\mathcal{P}' = \{p'_1, p'_2, \dots, p'_n\}$,
Initialization: Initial model: f_0 , initial mask: \mathcal{M}_0 ,

- 1: # Sequential tasks
- 2: **for** task $T_t \in \{T_1, T_2, \dots, T_{n+k}\}$ **do**
- 3: **if** $t = 1$ **then**
- 4: # First task
- 5: Train f_0 on \mathcal{D}_1 , get f_1 ;
- 6: Sequentially prune f_1 with ratios p_1 and p'_1 , get masks \mathcal{M}_1 and \mathcal{M}'_1 ;
- 7: Apply $\mathcal{M}_1, \mathcal{M}'_1$ to f_1 , successively, and fine-tune several epochs on \mathcal{D}_1 ;
- 8: Save f_1, \mathcal{M}_1 , and \mathcal{M}'_1 ;
- 9: **else if** $1 < t \leq n$ **then**
- 10: # Preset tasks
- 11: Apply Algorithm 2 to exploit the relevance between T_t and $\{T_1, T_2, \dots, T_{t-1}\}$, get f'_{t-1} ;
- 12: Train f'_{t-1} on \mathcal{D}_t , get f_t ;
- 13: Sequentially prune f_t with ratios p_t and p'_t , get masks \mathcal{M}_t and \mathcal{M}'_t ;
- 14: Apply $\mathcal{M}_t, \mathcal{M}'_t$ to f_t , successively, and fine-tune several epochs on \mathcal{D}_t ;
- 15: Save f_t, \mathcal{M}_t , and \mathcal{M}'_t ;
- 16: **else if** $n < t \leq n + k$ **then**
- 17: # Additional tasks
- 18: Apply Algorithm 2 to exploit the relevance between T_t and $\{T_1, T_2, \dots, T_{t-1}\}$, get f'_{t-1} ;
- 19: **if** $t = n + 1$ **then**
- 20: Initialize \mathcal{M}'_{t-1} to \mathcal{M}_t ;
- 21: **else**
- 22: Initialize \mathcal{M}_{t-1} to \mathcal{M}_t ;
- 23: **end if**
- 24: Apply \mathcal{M}_t to f'_{t-1} , then fine-tune several epochs on \mathcal{D}_t , get f_t ;
- 25: Save f_t and \mathcal{M}_t ;
- 26: **end if**
- 27: **end for**

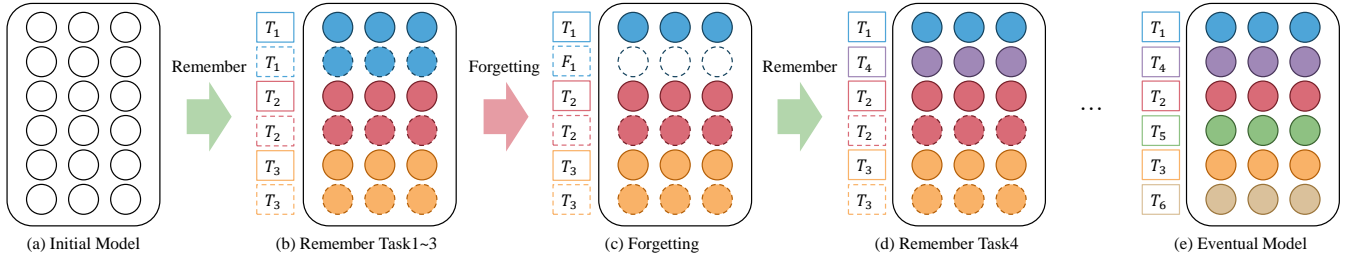


Fig. 2. The training process of SILF, where (a)-(b) belong to the preset stage and (c)-(d) belong to the additional stage. The numerous circles in those rounded rectangles indicate the parameters of the model. The circle's color corresponds to the task index it belongs to (e.g., blue corresponds to task 1). The dashed circles indicate that these parameters are available for the additional stage.

Algorithm 2 Task Relevance Guided Reuse Algorithm

Input: Current dataset: $\mathcal{D}_t = \{X_t, Y_t\}$,
 previous model: f_{t-1} , masks: $\{\mathcal{M}_1, \mathcal{M}_2, \dots, \mathcal{M}_{t-1}\}$,
 1: **for** $i \in \{1, 2, \dots, t-1\}$ **do**
 2: Apply \mathcal{M}_i to f_{t-1} , get $f_i = f_{t-1} \cdot \mathcal{M}_i$;
 3: Input X_t into f_i , get scores $S_{t,i} = f_i(X_t)$;
 4: Calculate $SRCC_{t,i}$;
 5: Calculate the reuse ratio $R_{t,i}$;
 6: Keep important parameters for T_t in T_i with a ratio of $R_{t,i}$, and prune the rest;
 7: **end for**

III. THE PROPOSED METHOD

A scalable incremental learning framework (SILF) for cross-task BIQA is proposed in this section. The training process of SILF can be divided into two stages, as shown in Fig. 2. The first is the preset stage. The initial model progressively remembers preset tasks, as shown in Fig. 2(a)-(b). With a sequentially remember and reuse strategy, our proposed network not only avoids the catastrophic forgetting problem in cross-task BIQA but also improves the performance of BIQA by selectively reusing some parameters of the learned tasks. The second is the additional stage, which is shown in Fig. 2(c)-(e). Thanks to the scalable learning strategy, our model can adapt to additional tasks by forgetting some of the parameters of the learned tasks.

Without loss of generality, our work follows a sequential task incremental learning setting, a familiar setting in incremental learning. The training details of SILF are summarized in Algorithm 1. The schematic diagram of a 4×4 filter update process in SILF during the training process is shown in Fig. 3. In the remainder of this section, we present our approach in the form of sequential tasks.

A. Remember Preset Tasks

Input and Initialization: Given initial model f_0 pre-trained on ImageNet [64], initial mask \mathcal{M}_0 filled with 1, and datasets \mathcal{D} . We pre-set the task capacity as n , the scalable task capacity as k , the first pruning ratios as \mathcal{P} , and the second pruning ratios as \mathcal{P}' . We divide \mathcal{D} into datasets of preset tasks $\{\mathcal{D}_t\}_{t=1}^n$ and datasets of additional tasks $\{\mathcal{D}_t\}_{t=n+1}^{n+k}$.

Task 1: First, we train f_0 on \mathcal{D}_1 and optimize all parameters of f_0 . The optimized model is defined as f_1 .

Second, we successively perform two sequential prunings on f_1 . The pruning ratio of the two prunings is set to p_1 and p'_1 respectively. We obtained masks \mathcal{M}_1 and \mathcal{M}'_1 after two pruning sessions.

Fig. 3(a) shows the change process of a filter during the training of T_1 . The left side of Fig. 3(a) shows the initial mask filled by 1, which belongs to \mathcal{M}_0 . The middle of Fig. 3(a) shows the result after the first pruning, which belongs to \mathcal{M}_1 , with the pruned part filled by 0. The right side of Fig. 3(a) is the result after the second pruning, which belongs to \mathcal{M}'_1 , part of the parameters belonging to T_1 is pruned, and the pruned part is changed from dark to light blue.

Take the first pruning process of a convolutional layer in f_1 as an example. We first sort all parameters of this layer by absolute value and then calculate the pruning threshold based on the pruning ratio p_1 . Parameters above the threshold are considered essential for T_1 , and the corresponding value in the mask is set to 1 (i.e., the current task index). Parameters below the threshold are considered unimportant for T_1 , and the corresponding value in the mask is set to 0. Similar operations are performed at each layer of f_1 to obtain \mathcal{M}_1 . The second pruning is done after the first, and the pruning process is similar to the first.

Third, we cyclically train the model after the first and second pruning. We first apply \mathcal{M}'_1 to f_1 and fine-tune several epochs on \mathcal{D}_1 , then apply \mathcal{M}_1 to f_1 and fine-tune several epochs on \mathcal{D}_1 . After several cycles of the above training steps, we obtain the scalable model f_1 . Finally, we save the fine-tuned model f_1 , masks \mathcal{M}_1 and \mathcal{M}'_1 .

Task t ($1 < t \leq n$): We call the learning stage of T_t ($1 < t \leq n$) the preset stage, denoted by S_P . Before the training of T_t , we apply Algorithm 2 to explore the relevance between T_t and $\{T_1, T_2, \dots, T_{t-1}\}$. For $T_i \in \{T_1, T_2, \dots, T_{t-1}\}$, we first apply \mathcal{M}_i to f_{t-1} :

$$f_i = f_{t-1} \cdot \mathcal{M}_i \quad (1)$$

then we input the training set of \mathcal{D}_t into f_i to obtain the prediction scores:

$$S_{t,i} = f_i(X_t) \quad (2)$$

where X_t is the training set of \mathcal{D}_t . Then $SRCC_{t,i}$ (Spearman Rank order Correlation Coefficient) is calculated based on

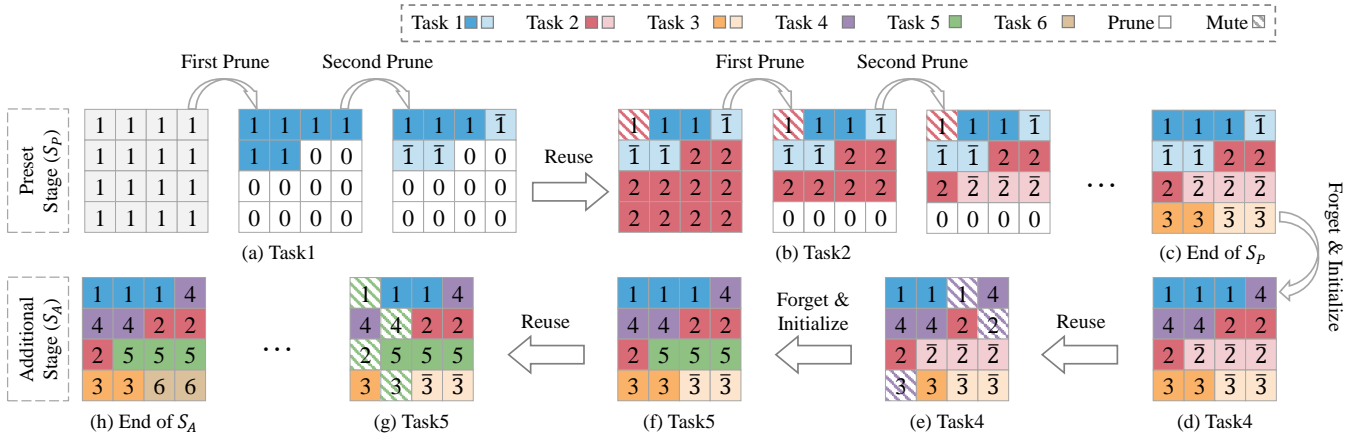


Fig. 3. The evolution of a 4×4 filter during training. Each square in the filter corresponds to a number. The number equal to 0 indicates that the parameters of the position are pruned, and the number not equal to 0 represents the task label. The shaded square in the figure indicates that the parameters at this position are not included in the calculation of the current task (i.e., "Mute").

predicted scores $S_{t,i}$ and ground truth scores Y_t . The reuse ratio between T_t and T_i is defined as:

$$R_{t,i} = \begin{cases} 1 + \lambda \cdot SRCC_{t,i}, & \text{if } SRCC_{t,i} < 0 \\ 1, & \text{otherwise.} \end{cases} \quad (3)$$

where λ is a constant, which we set to 0.5 in this paper. Equation (3) aims to quantify the parameter reuse ratio of one task by considering its relevance to another task. More specifically, we tend to increase the reuse ratio of the current task from relevant knowledge and decrease the reuse ratio of the current task from irrelevant knowledge. Since previous tasks' data are unavailable, we use the previous model's performance on current data, i.e., SRCC, to measure the task relevance in continual learning, where a better performance means higher task relevance and vice versa.

For each $T_i \in \{T_1, T_2, \dots, T_{t-1}\}$, T_t reuses the parameters belonging to T_i in proportion $R_{t,i}$, and the rest of the parameters belonging to T_i are muted. In the subsequent training of T_t , we temporarily ignore the muted part. The remaining training steps for T_t are similar to T_1 and will not be repeated here.

Fig. 3(b) shows the update process of the filter during the training of T_2 . Before the training of T_2 , we first apply Algorithm 2 to calculate the reuse ratio $R_{2,1}$ between T_2 and T_1 . Then we mute some parameters belonging to T_1 according to $R_{2,1}$ (shaded squares in Fig. 3(b) are muted). The next steps are similar to Task 1 and will not be repeated here.

B. Remember Additional Tasks by Forgetting

Task t ($n < t \leq n + k$): We call the learning stage of T_t ($n < t \leq n + k$) the additional stage, denoted by S_A . In preset stage S_P , the second pruned mask of T_t ($1 < t \leq n$) is saved as \mathcal{M}'_t . The locations of $mask = t$ and $mask = \bar{t}$ in \mathcal{M}'_t indicate that the parameters at these locations belong to T_t ($1 < t \leq n$), where the locations of $mask = \bar{t}$ indicate that the parameters corresponding to these locations can be used for subsequent additional tasks. In Fig. 3, dark and light squares of the same color belong to the same task, with light colors

indicating availability for subsequent additional tasks. Take Fig. 3(a) as an example, the dark blue squares correspond to $mask = 1$, and the light blue squares correspond to $mask = \bar{1}$.

Before the training of T_t ($n < t \leq n + k$), we first initialize \mathcal{M}_t by forgetting. Specifically, we initialize \mathcal{M}'_{t-1} to \mathcal{M}_t if $t = n + 1$, and we initialize \mathcal{M}_{t-1} to \mathcal{M}_t if $t > n + 1$. The initialization operation replaces the part of \mathcal{M}_{t-1} or \mathcal{M}'_{t-1} where $mask = \bar{t} - n$ is with $mask = t$. Fig. 3(c)-(d) show the initialization process of \mathcal{M}_4 before the training of T_4 . We initialize the part of \mathcal{M}'_3 with $mask = 1$ to $mask = 4$ so that we can utilize this part of the parameters to learn the additional T_4 .

Then we apply Algorithm 2 to explore the relevance between T_t ($n < t \leq n + k$) and $\{T_1, T_2, \dots, T_{t-1}\}$. The operation of calculating the reuse ratio is the same as T_t ($1 < t \leq n$). It is not repeated here. Finally, we apply \mathcal{M}_t to f_t and fine-tune it on \mathcal{D}_t . Fig. 3(h) shows the state of the mask at the end of S_A . After all the learning steps in this section, our proposed SILF completes the learning of S_P and S_A .

IV. EXPERIMENTAL RESULTS

In this section, we first describe the experimental setups, including IQA datasets, performance evaluation metrics, and implementation details. Then we compare the performance of the proposed with the state-of-the-art methods. Finally, we conduct a series of ablation studies to compare the performance of different settings.

A. Experimental Setups

1) **Datasets:** The main experiments are conducted on the following datasets:

Synthetically distorted datasets, including LIVE [65], CSIQ [66], LIVE-MD [67], TID2013 [68], and KADID-10k [69]. LIVE-MD consists of two multi-distortion datasets with a total of 450 distorted images. KADID-10k is a recently published large-scale synthetic database containing 81 reference images degraded by 25 distortion types in 5 levels for 10,125 distorted images.

TABLE I
SUMMARY OF IQA DATASETS USED IN OUR EXPERIMENTS

Dataset	Distort. Type	Content	# Distort. Types	# Distort. Images	Subjective Environment	Subjective Rating Type	Year
LIVE [65]	Synthetic	29	5	779	Laboratory	DMOS	2006
CSIQ [66]		30	6	866	Laboratory	DMOS	2010
LIVE-MD [67]		15	4	450	Laboratory	DMOS	2012
TID2013 [68]		25	24	3,000	Laboratory	MOS	2013
KADID-10k [69]		81	25	10,125	Crowdsourcing	MOS	2019
LIVE-CH [70]	Authentic	1,169	N/A	1,169	Crowdsourcing	MOS	2016
KONIQ-10k [71]		10,073	N/A	10,073	Crowdsourcing	MOS	2018
SPAQ [72]		11,125	N/A	11,125	Laboratory	MOS	2020
SHRQ-Aerial [73]	Enhanced	30	N/A	240	Laboratory	MOS	2019
SHRQ-Regular [73]		45	N/A	360	Laboratory	MOS	2019
IVIPC-DQA [74]		206	N/A	1,236	Laboratory	MOS	2019
LIEQ [75]		100	N/A	1,000	Laboratory	MOS	2021

Authentically distorted datasets, including LIVE-CH [70], KONIQ-10k [71], and SPAQ [72]. LIVE-CH contains 1162 images captured under highly diverse conditions by many camera devices. KONIQ-10k and SPAQ are two recently proposed large-scale datasets containing 10,073 and 11,125 authentic distortion images, respectively.

Enhancement distorted datasets including SHRQ [73], IVIPC-DQA [74], and LIEQ [75]. SHRQ contains two subsets, regular and aerial image subsets, respectively. We treat them as two separate datasets, denoted by SHRQ-A and SHRQ-R, respectively. IVIPC-DQA contains 1,236 derained images generated from 6 single image rain removal algorithms. LIEQ includes 1,000 light-enhanced images generated from 100 low-light images using 10 low-light image enhancement algorithms. Please refer to Table I for details of each dataset.

2) *Performance Evaluation Metrics*: We employ the commonly used metric SRCC [76] to evaluate BIQA performance. The larger the value of SRCC, the better the performance of BIQA. Following the criteria of [77], we evaluate the performance of cross-task BIQA from three perspectives: average accuracy, average forgetting, and average plasticity in the SRCC. Average accuracy is the average SRCC of all BIQA tasks at the end of their incremental learning process, which is defined as:

$$A_T = \frac{1}{T} \sum_{i=1}^T SRCC_{T,i} \quad (4)$$

Average forgetting measures how much information the model has forgotten about previous tasks, which is formulated as:

$$F_T = \frac{1}{T-1} \sum_{i=1}^{T-1} \max_{t \in \{1, \dots, T\}} (SRCC_{t,i} - SRCC_{T,i}) \quad (5)$$

Average plasticity aims to evaluate the ability of the model to adapt to new tasks, which is defined as:

$$P_T = \frac{1}{T} \sum_{i=1}^T SRCC_{i,i} \quad (6)$$

where T is the total number of learned tasks, $SRCC_{m,n}$ is the SRCC of the n_{th} task after learning the first m tasks sequentially.

3) *Implementation Details*: Our proposed SILF is implemented with the PyTorch library. All experiments are executed on Ubuntu 18.04 with i9-9900k CPU and two NVIDIA GTX TITAN XP GPUs. We utilize ResNeXt101 [78] as the backbone network of our SILF, and we replace the last two fully connected layers of ResNeXt101 with one fully connected layer of size [2048, 1]. The parameters of the backbone network are initialized by the weights pre-trained on ImageNet [64]. We add a sigmoid activation function after the fully connected layer to make the score output by the network in the range [0, 1]. We set the number of preset and additional tasks to 3 and the first and second pruning ratios to [0.7, 0.5, 0] and [0.4, 0.4, 0.4], respectively. We adopt the L_1 loss as the loss function for each task and apply stochastic gradient descent (SGD) as the optimizer. We set the initial learning rate to 1×10^{-3} with a decay factor of 0.5 for every 10 epochs. Following previous works [31], [34], we split 80% of each dataset into training sets and the remaining 20% into test sets without using validation sets. We stop training at a preset 40 epoch. During training, we crop each image into five 256×256 patches (center and four corners) and take the average score of these patches as the final score for this image. Following the similar setting of [14], we repeat the random split three times on each database and report the average SRCC result across all trials.

B. Comparison Methods

We compared six methods, including two benchmarks and four incremental learning strategies. The same backbone network is applied to each method for a fair comparison. The detailed settings of these methods are presented in the following:

- **Separate Learning (SL)**: Each task is trained with an independent model. The results are usually considered an upper bound on the performance of BIQA.
- **NO Remember Learning (NO-RL)**: Retrain new tasks directly on the old model, where all tasks share all parameters of the same model. This approach usually leads to catastrophic forgetting.
- **NO Relevance Reuse (NO-RR)**: We set the value of λ in (3) to 0. In this setting, the relevance between tasks is

TABLE II
CROSS-TASK BIQA PERFORMANCE COMPARISON (AVERAGE ACCURACY) ON TASK SEQUENCE I

Method	Tasks						Mean
	1 st (LIVE-CH)	2 nd (CSIQ)	3 rd (LIEQ)	4 th (KONIQ)	5 th (LIVE-MD)	6 th (SHRQ-A)	
SL	0.8529	0.8953	0.8990	0.8990	0.9105	0.9191	0.8960
LWF	0.8260	0.3796	0.3565	0.4025	0.3543	0.2989	0.4363
PNN	0.6809	0.3159	0.2640	0.3764	0.2726	0.3044	0.3690
R&R-Net (3 tasks)	0.8163	0.8665	0.8667	/	/	/	/
R&R-Net (6 tasks)	0.7910	0.8359	0.8560	0.8594	0.8206	0.8252	0.8314
NO-RL	0.8039	0.4663	0.4455	0.4001	0.4008	0.2775	0.4657
NO-RR	0.8494	0.8786	0.8694	0.8389	0.8591	0.8420	0.8562
Proposed (SILF)	0.8472	0.8779	0.8680	0.8569	0.8765	0.8645	0.8652

TABLE III
CROSS-TASK BIQA PERFORMANCE COMPARISON (AVERAGE ACCURACY) ON TASK SEQUENCE II

Method	Tasks						Mean
	1 st (LIVE)	2 nd (SPAQ)	3 rd (KADID)	4 th (IVIPC-DQA)	5 th (TID2013)	6 th (SHRQ-R)	
SL	0.9711	0.9420	0.9131	0.8366	0.8342	0.8364	0.8889
LWF	0.9628	0.2654	0.2292	0.2544	0.2497	0.2973	0.3765
PNN	0.8853	0.0796	0.2355	0.1997	0.2734	0.2673	0.3235
R&R-Net (3 tasks)	0.9577	0.9356	0.8967	/	/	/	/
R&R-Net (6 tasks)	0.9452	0.9275	0.9014	0.7383	0.7281	0.7260	0.8277
NO-RL	0.9663	0.2073	0.2813	0.2844	0.3733	0.4253	0.4230
NO-RR	0.9576	0.9349	0.9081	0.7907	0.7823	0.7747	0.8580
Proposed (SILF)	0.9610	0.9339	0.9065	0.8094	0.7924	0.7914	0.8658

not considered during training. The rest are the same as SILF.

- Learning without Forgetting (LwF) [42]: LWF incorporates knowledge distillation and fine-tuning to learn new tasks while retaining outputs of old tasks. For each new task, we add 256 neurons to the penultimate fully connected layer of the network.
- Progressive Neural Networks (PNN) [53]: PNN keeps a library of models during training and adds lateral connections between models to extract features useful for new tasks. We add a branch for each new task and use lateral connections between branches.
- Remember and Reuse Network (R&R-Net) [15]: We assign parameters equally to each task. It is worth noting that this method requires us to set the number of tasks in advance. In practice, R&R-Net is unable to learn additional tasks.

C. Main Results

To evaluate the cross-task BIQA performance of different methods, we divide the twelve tasks into two task sequences and conduct experiments on them. Tables II and III show the average accuracy results for Sequence I and Sequence II, respectively. The results in Tables II and III first row are for separate learning (SL), which is usually considered the upper bound of BIQA performance and is marked in bold. In addition, we employ red and blue fonts to indicate the first and second ranking of performance among the remaining methods, respectively.

There are several valuable findings from the analysis of Tables II and III. First, NO-RL performance on learned tasks decreased significantly with the sequential learning process

due to the inability to remember learned tasks (i.e., experienced catastrophic forgetting during incremental learning). Second, LWF and PNN are usually used for classification scenarios that are relatively similar between tasks. The cross-task BIQA results of LWF and PNN are unsatisfactory due to the significant differences among tasks in cross-task BIQA. Third, R&RNet shows a remarkable ability to avoid forgetting. Still, its average accuracy on multiple tasks is lower than NO-RR and SILF because it employs only fixed first pruning. Last, our proposed SILF can effectively exploit the inter-task relevance information to improve the performance of cross-task BIQA compared to NO-RR. In Tables II and III, the mean values of SILF average accuracy are improved by 1.05% and 0.91% compared to NO-RR.

Table IV shows the cross-task BIQA results for task sequence I. The second and third columns in Table IV show the sequential training datasets and the comparison methods, respectively. The model for each method was tested on all learned tasks as each new task was completed. The test results are SRCC values, as shown in Table IV. The second row of Table IV shows the results of separate learning (SL), which can be considered an upper bound on the performance of each task. Rows 3-9 in Table IV show the results of each method learned sequentially and tested on learned tasks.

D. Ablation Experiments

In this subsection, we conduct a series of ablation experiments to evaluate the factors that affect the performance of our method.

1) *The Impact of Training Order*: To evaluate the robustness of our method to the training order, we adjusted the order of the tasks in Sequence I. Sequence I contains two tasks

TABLE IV
CROSS-TASK BIQA PERFORMANCE COMPARISON (SRCC) ON TASK SEQUENCE I

Sequence	Dataset	Method	LIVE-CH	CSIQ	LIEQ	KONIQ	LIVE-MD	SHRQ-A
-	All	SL	0.8529	0.9377	0.9064	0.8991	0.9564	0.9620
1 st	LIVE-CH	LWF	0.8260	-	-	-	-	-
		PNN	0.6809	-	-	-	-	-
		R&R-Net	0.7910	-	-	-	-	-
		NO-RL	0.8039	-	-	-	-	-
		NO-RR	0.8494	-	-	-	-	-
		Proposed (SILF)	0.8472	-	-	-	-	-
2 nd	CSIQ	LWF	0.6621	0.0971	-	-	-	-
		PNN	-0.1681	0.7998	-	-	-	-
		R&R-Net	0.7910	0.8807	-	-	-	-
		NO-RL	0.0668	0.8658	-	-	-	-
		NO-RR	0.8494	0.9077	-	-	-	-
		Proposed (SILF)	0.8472	0.9086	-	-	-	-
3 rd	LIEQ	LWF	0.6599	-0.2293	0.6389	-	-	-
		PNN	0.0446	0.1965	0.5510	-	-	-
		R&R-Net	0.7910	0.8807	0.8963	-	-	-
		NO-RL	0.1920	0.2592	0.8852	-	-	-
		NO-RR	0.8494	0.9077	0.8512	-	-	-
		Proposed (SILF)	0.8472	0.9086	0.8481	-	-	-
4 th	KONIQ	LWF	0.7706	-0.5298	0.6326	0.7365	-	-
		PNN	0.7428	-0.6403	0.5367	0.8665	-	-
		R&R-Net	0.7910	0.8807	0.8963	0.8694	-	-
		NO-RL	0.7973	-0.7429	0.6487	0.8973	-	-
		NO-RR	0.7929	0.8880	0.7830	0.8916	-	-
		Proposed (SILF)	0.8045	0.8984	0.8343	0.8902	-	-
5 th	LIVE-MD	LWF	0.6347	0.1613	0.3391	0.5302	0.1060	-
		PNN	0.1820	0.4289	0.1869	0.1097	0.4556	-
		R&R-Net	0.7910	0.8807	0.8963	0.8694	0.6657	-
		NO-RL	0.2769	0.5638	-0.1346	0.3627	0.9354	-
		NO-RR	0.7929	0.8880	0.7830	0.8916	0.9402	-
		Proposed (SILF)	0.8045	0.8984	0.8343	0.8902	0.9553	-
6 th	SHRQ-A	LWF	0.6280	-0.2274	0.4695	0.5440	-0.3616	0.7411
		PNN	0.3803	-0.2211	0.5078	0.4398	-0.0952	0.8145
		R&R-Net	0.7910	0.8807	0.8963	0.8694	0.6657	0.8478
		NO-RL	0.5931	-0.7045	0.5703	0.5866	-0.2739	0.8935
		NO-RR	0.7929	0.8880	0.7830	0.8916	0.9402	0.7565
		Proposed (SILF)	0.8045	0.8984	0.8343	0.8902	0.9553	0.8045

TABLE V
DIFFERENT TRAINING ORDERS. A, S, AND E ARE ACRONYMS FOR AUTHENTIC, SYNTHETIC, AND ENHANCEMENT RESPECTIVELY

Order	1 st	2 nd	3 rd	4 th	5 th	6 th
I	A (LIVE-CH)	S (CSIQ)	E (LIEQ)	A (KONIQ)	S (LIVE-MD)	E (SHRQ-A)
II	A (LIVE-CH)	E (LIEQ)	S (CSIQ)	A (KONIQ)	E (SHRQ-A)	S (LIVE-MD)
III	S (CSIQ)	A (LIVE-CH)	E (LIEQ)	S (LIVE-MD)	A (KONIQ)	E (SHRQ-A)
IV	S (CSIQ)	E (LIEQ)	A (LIVE-CH)	S (LIVE-MD)	E (SHRQ-A)	A (KONIQ)
V	E (LIEQ)	A (LIVE-CH)	S (CSIQ)	E (SHRQ-A)	A (KONIQ)	S (LIVE-MD)
VI	E (LIEQ)	S (CSIQ)	A (LIVE-CH)	E (SHRQ-A)	S (LIVE-MD)	A (KONIQ)

for each of the three task types. Please refer to Table I for the specific distortion type of each task. By permuting three different distortion types, we obtained six different training orders for Sequence I, as shown in Table V.

Table VI reports the results of the ablation experiments with different training orders. Each metric’s best and worst values are marked in red and blue, respectively. We apply the range of fluctuations and standard deviations to measure the robustness of our proposed model to the training order. The difference between the three metrics’ maximum and minimum values are 0.0256, 0.0179, and 0.0114, and their standard deviations are 0.0094, 0.0076, and 0.0042, respectively. We can infer from the above analysis that our proposed model is insensitive to

TABLE VI
ABLATION EXPERIMENTAL RESULTS ABOUT THE TRAINING ORDER

Training Order	Average Accuracy	Average Plasticity	Average Forgetting
I	0.8652	0.8757	0.0104
II	0.8698	0.8686	0.0077
III	0.8651	0.8578	0.0186
IV	0.8685	0.8594	0.0072
V	0.8442	0.8667	0.0087
VI	0.8606	0.8754	0.0088

the training order and has high robustness.

TABLE VII

ABLATION EXPERIMENTAL RESULTS ABOUT THE SECOND PRUNING RATIO

Second Pruning Ratio	Average Accuracy	Average Plasticity	Average Forgetting
0.1	0.8562	0.7935	0.0029
0.2	0.8662	0.8366	0.0035
0.3	0.8632	0.8498	0.0051
0.4 (SILF)	0.8652	0.8757	0.0104
0.5	0.8514	0.8748	0.0301
0.6	0.6633	0.8855	0.3326
0.7	-	-	-

TABLE VIII

ABLATION EXPERIMENTAL RESULTS ABOUT THE RELEVANT CONSTANT

Relevant Constant	Average Accuracy	Average Plasticity	Average Forgetting
0 (NO-RR)	0.8562	0.8661	0.0226
0.1	0.8636	0.8614	0.0117
0.3	0.8547	0.8474	0.0078
0.5 (SILF)	0.8652	0.8757	0.0104
0.7	0.8564	0.8752	0.0125
0.9	0.8183	0.8737	0.0714

2) *The Impact of Second Pruning Ratio:* Table VII shows the performance of our proposed model under different second pruning ratio settings. The top three values of each metric are marked in red, green, and blue.

We can summarize the following points from Table VII. First, the average accuracy takes higher values at second pruning ratios of 0.2, 0.3, and 0.4, decreasing significantly when the second pruning ratio is 0.6. When the second pruning ratio is 0.7, the model cannot infer due to insufficient remaining parameters. Second, average plasticity and average forgetting were positively correlated with the second pruning ratio. Considering the two points mentioned above, we take 0.4 as the second pruning ratio of our proposed model.

3) *The Impact of Relevant Constant:* Here, we evaluate the effect of λ in (3). Table VIII demonstrates the performance of our proposed model under different relevant constant settings. The top three values of each metric are marked in red, green, and blue.

Table VIII shows that the average accuracy and average plasticity metrics are both highest at a relevant constant of 0.5, and the average forgetting metric is the second highest. In addition, our proposed SILF improves by approximately 1.05%, 1.11%, and 1.22% for the three metrics, respectively, compared to the relevant constant taking a value of 0 (i.e., NO-RR).

V. CONCLUSION

The R&R-Net proposed in our previous work addresses catastrophic forgetting in cross-task BIQA. However, R&R-Net cannot learn additional tasks due to a rigid parameter assignment strategy. This paper presents a scalable incremental learning framework (SILF) to extend R&R-Net by utilizing a scalable incremental learning strategy. Specifically, by gradually and selectively pruning unimportant neurons from

previously settled parameter subsets, we develop a scalable memory unit, which enables us to forget part of previous experiences and free the limited memory capacity for adapting to emerging new tasks. Extensive experiments on eleven IQA datasets demonstrate that our proposed method significantly outperforms the other state-of-the-art methods in cross-task BIQA.

REFERENCES

- [1] W. Zhang, J. Yan, S. Hu, Y. Ma, and D. Deng, "Predicting perceptual quality of images in realistic scenario using deep filter banks," *Journal of Electronic Imaging*, vol. 27, no. 2, p. 023037, 2018.
- [2] W. Zhang, K. Ma, G. Zhai, and X. Yang, "Learning to blindly assess image quality in the laboratory and wild," in *2020 IEEE International Conference on Image Processing (ICIP)*. IEEE, 2020, pp. 111–115.
- [3] Q. Jiang, F. Shao, W. Lin, K. Gu, G. Jiang, and H. Sun, "Optimizing multi-stage discriminative dictionaries for blind image quality assessment," *IEEE Transactions on Multimedia*, vol. 20, no. 8, pp. 2035–2048, 2017.
- [4] S. Yang, Q. Jiang, W. Lin, and Y. Wang, "Sgdnnet: An end-to-end saliency-guided deep neural network for no-reference image quality assessment," in *Proceedings of the 27th ACM International Conference on Multimedia*, 2019, pp. 1383–1391.
- [5] Q. Jiang, Z. Liu, K. Gu, F. Shao, X. Zhang, H. Liu, and W. Lin, "Single image super-resolution quality assessment: a real-world dataset, subjective studies, and an objective metric," *IEEE Transactions on Image Processing*, vol. 31, pp. 2279–2294, 2022.
- [6] Q. Jiang, Y. Gu, C. Li, R. Cong, and F. Shao, "Underwater image enhancement quality evaluation: Benchmark dataset and objective metric," *IEEE Transactions on Circuits and Systems for Video Technology*, 2022.
- [7] Q. Jiang, F. Shao, W. Lin, and G. Jiang, "Blique-tmi: Blind quality evaluator for tone-mapped images based on local and global feature analyses," *IEEE Transactions on Circuits and Systems for Video Technology*, vol. 29, no. 2, pp. 323–335, 2017.
- [8] J. Xu, W. Zhou, H. Li, F. Li, and Q. Jiang, "Quality assessment of multi-exposure image fusion by synthesizing local and global intermediate references," *Displays*, vol. 74, p. 102188, 2022.
- [9] G. Zhai, Y. Zhu, and X. Min, "Comparative perceptual assessment of visual signals using free energy features," *IEEE Transactions on Multimedia*, vol. 23, pp. 3700–3713, 2020.
- [10] Y. Huang, H. Xu, and Z. Ye, "Image quality evaluation for oled-based smart-phone displays at various lighting conditions," *Displays*, vol. 70, p. 102115, 2021.
- [11] M. McCloskey and N. J. Cohen, "Catastrophic interference in connectionist networks: The sequential learning problem," in *Psychology of learning and motivation*. Elsevier, 1989, vol. 24, pp. 109–165.
- [12] W. Zhang, K. Ma, G. Zhai, and X. Yang, "Task-specific normalization for continual learning of blind image quality models," *arXiv preprint arXiv:2107.13429*, 2021.
- [13] W. Zhang, D. Li, C. Ma, G. Zhai, X. Yang, and K. Ma, "Continual learning for blind image quality assessment," *IEEE Transactions on Pattern Analysis and Machine Intelligence*, 2022.
- [14] J. Liu, W. Zhou, X. Li, J. Xu, and Z. Chen, "Liq: Lifelong blind image quality assessment," *IEEE Transactions on Multimedia*, 2022.
- [15] R. Ma, H. Luo, Q. Wu, K. N. Ngan, H. Li, F. Meng, and L. Xu, "Remember and reuse: Cross-task blind image quality assessment via relevance-aware incremental learning," in *Proceedings of the 29th ACM International Conference on Multimedia*, 2021, pp. 5248–5256.
- [16] K. Gu, G. Zhai, X. Yang, and W. Zhang, "Using free energy principle for blind image quality assessment," *IEEE Transactions on Multimedia*, vol. 17, no. 1, pp. 50–63, 2014.
- [17] Q. Li, W. Lin, J. Xu, and Y. Fang, "Blind image quality assessment using statistical structural and luminance features," *IEEE Transactions on Multimedia*, vol. 18, no. 12, pp. 2457–2469, 2016.
- [18] K. Gu, S. Wang, G. Zhai, S. Ma, X. Yang, W. Lin, W. Zhang, and W. Gao, "Blind quality assessment of tone-mapped images via analysis of information, naturalness, and structure," *IEEE Transactions on Multimedia*, vol. 18, no. 3, pp. 432–443, 2016.
- [19] Y. Zhan, R. Zhang, and Q. Wu, "A structural variation classification model for image quality assessment," *IEEE Transactions on Multimedia*, vol. 19, no. 8, pp. 1837–1847, 2017.
- [20] Q. Wu, H. Li, Z. Wang, F. Meng, B. Luo, W. Li, and K. N. Ngan, "Blind image quality assessment based on rank-order regularized regression," *IEEE Transactions on Multimedia*, vol. 19, no. 11, pp. 2490–2504, 2017.

- [21] A. K. Moorthy and A. C. Bovik, "Blind image quality assessment: From natural scene statistics to perceptual quality," *IEEE transactions on Image Processing*, vol. 20, no. 12, pp. 3350–3364, 2011.
- [22] M. A. Saad, A. C. Bovik, and C. Charrier, "Blind image quality assessment: A natural scene statistics approach in the dct domain," *IEEE transactions on Image Processing*, vol. 21, no. 8, pp. 3339–3352, 2012.
- [23] A. Mittal, A. K. Moorthy, and A. C. Bovik, "No-reference image quality assessment in the spatial domain," *IEEE Transactions on image processing*, vol. 21, no. 12, pp. 4695–4708, 2012.
- [24] P. Ye, J. Kumar, L. Kang, and D. Doermann, "Unsupervised feature learning framework for no-reference image quality assessment," in *2012 IEEE conference on computer vision and pattern recognition*. IEEE, 2012, pp. 1098–1105.
- [25] P. Zhang, W. Zhou, L. Wu, and H. Li, "Som: Semantic obviousness metric for image quality assessment," in *Proceedings of the IEEE Conference on Computer Vision and Pattern Recognition*, 2015, pp. 2394–2402.
- [26] L. Kang, P. Ye, Y. Li, and D. Doermann, "Convolutional neural networks for no-reference image quality assessment," in *Proceedings of the IEEE conference on computer vision and pattern recognition*, 2014, pp. 1733–1740.
- [27] J. Kim and S. Lee, "Fully deep blind image quality predictor," *IEEE Journal of selected topics in signal processing*, vol. 11, no. 1, pp. 206–220, 2016.
- [28] S. Bosse, D. Maniry, K.-R. Müller, T. Wiegand, and W. Samek, "Deep neural networks for no-reference and full-reference image quality assessment," *IEEE Transactions on image processing*, vol. 27, no. 1, pp. 206–219, 2017.
- [29] B. Bare, K. Li, and B. Yan, "An accurate deep convolutional neural networks model for no-reference image quality assessment," in *2017 IEEE International Conference on Multimedia and Expo (ICME)*. IEEE, 2017, pp. 1356–1361.
- [30] J. Guan, S. Yi, X. Zeng, W.-K. Cham, and X. Wang, "Visual importance and distortion guided deep image quality assessment framework," *IEEE Transactions on Multimedia*, vol. 19, no. 11, pp. 2505–2520, 2017.
- [31] W. Zhang, K. Ma, J. Yan, D. Deng, and Z. Wang, "Blind image quality assessment using a deep bilinear convolutional neural network," *IEEE Transactions on Circuits and Systems for Video Technology*, vol. 30, no. 1, pp. 36–47, 2018.
- [32] D. Yang, V.-T. Peltoketo, and J.-K. Kamarainen, "Cnn-based cross-dataset no-reference image quality assessment," in *Proceedings of the IEEE/CVF International Conference on Computer Vision Workshops*, 2019, pp. 0–0.
- [33] H. Zhu, L. Li, J. Wu, W. Dong, and G. Shi, "Metaqa: Deep meta-learning for no-reference image quality assessment," in *Proceedings of the IEEE/CVF Conference on Computer Vision and Pattern Recognition*, 2020, pp. 14 143–14 152.
- [34] S. Su, Q. Yan, Y. Zhu, C. Zhang, X. Ge, J. Sun, and Y. Zhang, "Blindly assess image quality in the wild guided by a self-adaptive hyper network," in *Proceedings of the IEEE/CVF Conference on Computer Vision and Pattern Recognition*, 2020, pp. 3667–3676.
- [35] K. He, X. Zhang, S. Ren, and J. Sun, "Deep residual learning for image recognition," in *Proceedings of the IEEE conference on computer vision and pattern recognition*, 2016, pp. 770–778.
- [36] K. Simonyan and A. Zisserman, "Very deep convolutional networks for large-scale image recognition," *arXiv preprint arXiv:1409.1556*, 2014.
- [37] C. Finn, P. Abbeel, and S. Levine, "Model-agnostic meta-learning for fast adaptation of deep networks," in *International conference on machine learning*. PMLR, 2017, pp. 1126–1135.
- [38] A. Mittal, R. Soundararajan, and A. C. Bovik, "Making a "completely blind" image quality analyzer," *IEEE Signal processing letters*, vol. 20, no. 3, pp. 209–212, 2012.
- [39] L. Zhang, L. Zhang, and A. C. Bovik, "A feature-enriched completely blind image quality evaluator," *IEEE Transactions on Image Processing*, vol. 24, no. 8, pp. 2579–2591, 2015.
- [40] Q. Wu, Z. Wang, and H. Li, "A highly efficient method for blind image quality assessment," in *2015 IEEE International Conference on Image Processing (ICIP)*. IEEE, 2015, pp. 339–343.
- [41] Y. Liu, K. Gu, X. Li, and Y. Zhang, "Blind image quality assessment by natural scene statistics and perceptual characteristics," *ACM Transactions on Multimedia Computing, Communications, and Applications (TOMM)*, vol. 16, no. 3, pp. 1–91, 2020.
- [42] Z. Li and D. Hoiem, "Learning without forgetting," *IEEE transactions on pattern analysis and machine intelligence*, vol. 40, no. 12, pp. 2935–2947, 2017.
- [43] G. Hinton, O. Vinyals, J. Dean *et al.*, "Distilling the knowledge in a neural network," *arXiv preprint arXiv:1503.02531*, vol. 2, no. 7, 2015.
- [44] J. Kirkpatrick, R. Pascanu, N. Rabinowitz, J. Veness, G. Desjardins, A. A. Rusu, K. Milan, J. Quan, T. Ramalho, A. Grabska-Barwinska *et al.*, "Overcoming catastrophic forgetting in neural networks," *Proceedings of the national academy of sciences*, vol. 114, no. 13, pp. 3521–3526, 2017.
- [45] J. Schwarz, W. Czarnecki, J. Luketina, A. Grabska-Barwinska, Y. W. Teh, R. Pascanu, and R. Hadsell, "Progress & compress: A scalable framework for continual learning," in *International Conference on Machine Learning*. PMLR, 2018, pp. 4528–4537.
- [46] S.-A. Rebuffi, A. Kolesnikov, G. Sperl, and C. H. Lampert, "icarl: Incremental classifier and representation learning," in *Proceedings of the IEEE conference on Computer Vision and Pattern Recognition*, 2017, pp. 2001–2010.
- [47] E. Belouadah and A. Popescu, "Il2m: Class incremental learning with dual memory," in *Proceedings of the IEEE/CVF International Conference on Computer Vision*, 2019, pp. 583–592.
- [48] Y. Liu, Y. Su, A.-A. Liu, B. Schiele, and Q. Sun, "Mnemonics training: Multi-class incremental learning without forgetting," in *Proceedings of the IEEE/CVF conference on Computer Vision and Pattern Recognition*, 2020, pp. 12 245–12 254.
- [49] H. Shin, J. K. Lee, J. Kim, and J. Kim, "Continual learning with deep generative replay," *Advances in neural information processing systems*, vol. 30, 2017.
- [50] C. Wu, L. Herranz, X. Liu, J. van de Weijer, B. Raducanu *et al.*, "Memory replay gans: Learning to generate new categories without forgetting," *Advances in Neural Information Processing Systems*, vol. 31, 2018.
- [51] Y. Xiang, Y. Fu, P. Ji, and H. Huang, "Incremental learning using conditional adversarial networks," in *Proceedings of the IEEE/CVF International Conference on Computer Vision*, 2019, pp. 6619–6628.
- [52] I. Goodfellow, J. Pouget-Abadie, M. Mirza, B. Xu, D. Warde-Farley, S. Ozair, A. Courville, and Y. Bengio, "Generative adversarial nets," *Advances in neural information processing systems*, vol. 27, 2014.
- [53] A. A. Rusu, N. C. Rabinowitz, G. Desjardins, H. Soyer, J. Kirkpatrick, K. Kavukcuoglu, R. Pascanu, and R. Hadsell, "Progressive neural networks," *arXiv preprint arXiv:1606.04671*, 2016.
- [54] J. Yoon, E. Yang, J. Lee, and S. J. Hwang, "Lifelong learning with dynamically expandable networks," *arXiv preprint arXiv:1708.01547*, 2017.
- [55] C.-Y. Hung, C.-H. Tu, C.-E. Wu, C.-H. Chen, Y.-M. Chan, and C.-S. Chen, "Compacting, picking and growing for unforgetting continual learning," *Advances in Neural Information Processing Systems*, vol. 32, 2019.
- [56] X. Li, Y. Zhou, T. Wu, R. Socher, and C. Xiong, "Learn to grow: A continual structure learning framework for overcoming catastrophic forgetting," in *International Conference on Machine Learning*. PMLR, 2019, pp. 3925–3934.
- [57] J. Rajasegaran, M. Hayat, S. H. Khan, F. S. Khan, and L. Shao, "Random path selection for continual learning," *Advances in Neural Information Processing Systems*, vol. 32, 2019.
- [58] P. Singh, V. K. Verma, P. Mazumder, L. Carin, and P. Rai, "Calibrating cnns for lifelong learning," *Advances in Neural Information Processing Systems*, vol. 33, pp. 15 579–15 590, 2020.
- [59] C. Fernando, D. Banarse, C. Blundell, Y. Zwols, D. Ha, A. A. Rusu, A. Pritzel, and D. Wierstra, "Pathnet: Evolution channels gradient descent in super neural networks," *arXiv preprint arXiv:1701.08734*, 2017.
- [60] J. Serra, D. Suris, M. Miron, and A. Karatzoglou, "Overcoming catastrophic forgetting with hard attention to the task," in *International Conference on Machine Learning*. PMLR, 2018, pp. 4548–4557.
- [61] A. Mallya and S. Lazebnik, "Packnet: Adding multiple tasks to a single network by iterative pruning," in *Proceedings of the IEEE conference on Computer Vision and Pattern Recognition*, 2018, pp. 7765–7773.
- [62] A. Mallya, D. Davis, and S. Lazebnik, "Piggyback: Adapting a single network to multiple tasks by learning to mask weights," in *Proceedings of the European Conference on Computer Vision (ECCV)*, 2018, pp. 67–82.
- [63] S. Ebrahimi, M. Elhoseiny, T. Darrell, and M. Rohrbach, "Uncertainty-guided continual learning with bayesian neural networks," *arXiv preprint arXiv:1906.02425*, 2019.
- [64] J. Deng, W. Dong, R. Socher, L.-J. Li, K. Li, and L. Fei-Fei, "Imagenet: A large-scale hierarchical image database," in *2009 IEEE conference on computer vision and pattern recognition*. Ieee, 2009, pp. 248–255.
- [65] H. R. Sheikh, M. F. Sabir, and A. C. Bovik, "A statistical evaluation of recent full reference image quality assessment algorithms," *IEEE Transactions on image processing*, vol. 15, no. 11, pp. 3440–3451, 2006.

- [66] E. C. Larson and D. M. Chandler, "Most apparent distortion: full-reference image quality assessment and the role of strategy," *Journal of electronic imaging*, vol. 19, no. 1, p. 011006, 2010.
- [67] D. Jayaraman, A. Mittal, A. K. Moorthy, and A. C. Bovik, "Objective quality assessment of multiply distorted images," in *2012 Conference record of the forty sixth asilomar conference on signals, systems and computers (ASILOMAR)*. IEEE, 2012, pp. 1693–1697.
- [68] N. Ponomarenko, O. Ieremeiev, V. Lukin, K. Egiazarian, L. Jin, J. Astola, B. Vozel, K. Chehdi, M. Carli, F. Battisti *et al.*, "Color image database tid2013: Peculiarities and preliminary results," in *European workshop on visual information processing (EUVIP)*. IEEE, 2013, pp. 106–111.
- [69] H. Lin, V. Hosu, and D. Saupe, "Kadid-10k: A large-scale artificially distorted iqa database," in *2019 Eleventh International Conference on Quality of Multimedia Experience (QoMEX)*. IEEE, 2019, pp. 1–3.
- [70] D. Ghadiyaram and A. C. Bovik, "Massive online crowdsourced study of subjective and objective picture quality," *IEEE Transactions on Image Processing*, vol. 25, no. 1, pp. 372–387, 2015.
- [71] V. Hosu, H. Lin, T. Sziranyi, and D. Saupe, "Koniq-10k: An ecologically valid database for deep learning of blind image quality assessment," *IEEE Transactions on Image Processing*, vol. 29, pp. 4041–4056, 2020.
- [72] Y. Fang, H. Zhu, Y. Zeng, K. Ma, and Z. Wang, "Perceptual quality assessment of smartphone photography," in *Proceedings of the IEEE/CVF Conference on Computer Vision and Pattern Recognition*, 2020, pp. 3677–3686.
- [73] X. Min, G. Zhai, K. Gu, Y. Zhu, J. Zhou, G. Guo, X. Yang, X. Guan, and W. Zhang, "Quality evaluation of image dehazing methods using synthetic hazy images," *IEEE Transactions on Multimedia*, vol. 21, no. 9, pp. 2319–2333, 2019.
- [74] Q. Wu, L. Wang, K. N. Ngan, H. Li, and F. Meng, "Beyond synthetic data: A blind deraining quality assessment metric towards authentic rain image," in *2019 IEEE International Conference on Image Processing (ICIP)*. IEEE, 2019, pp. 2364–2368.
- [75] G. Zhai, W. Sun, X. Min, and J. Zhou, "Perceptual quality assessment of low-light image enhancement," *ACM Transactions on Multimedia Computing, Communications, and Applications (TOMM)*, vol. 17, no. 4, pp. 1–24, 2021.
- [76] Q. Wu, H. Li, F. Meng, and K. N. Ngan, "A perceptually weighted rank correlation indicator for objective image quality assessment," *IEEE Transactions on Image Processing*, vol. 27, no. 5, pp. 2499–2513, 2018.
- [77] D. Lopez-Paz and M. Ranzato, "Gradient episodic memory for continual learning," *Advances in neural information processing systems*, vol. 30, 2017.
- [78] S. Xie, R. Girshick, P. Dollár, Z. Tu, and K. He, "Aggregated residual transformations for deep neural networks," in *Proceedings of the IEEE conference on computer vision and pattern recognition*, 2017, pp. 1492–1500.